water

MDPI

Article

FeOOH-Modified Volcanic Rock for Ammonia Nitrogen Removal from Aqueous Solution: Adsorption Mechanism and Application Potential

Xuan Ru, Yang Liu, Jing Huang, Jiawei Chen, Zhilan Tian and Deqing Mo *

School of Life and Environmental Sciences, Guilin University of Electronic Technology, Guilin 541004, China; ruxuan121@guet.edu.cn (X.R.)
* Correspondence: modq@guet.edu.cn

Abstract

The use of volcanic rock, a typical soil amendment, to capture ammonia nitrogen from wastewater offers a promising route for nitrogen resource recovery. However, its low adsorption capacity remains a key limitation. In this study, hydroxylated iron oxide (FeOOH) was loaded onto volcanic rock via co-precipitation to obtain volcanic rock@FeOOH. Batch adsorption experiments showed that volcanic rock@FeOOH exhibited a significantly enhanced NH_4^+-N adsorption capacity (3.690 mg·g^{-1}) compared to volcanic rock (1.817 mg·g^{-1}). The adsorption process followed the Freundlich isotherm and pseudo-second-order kinetic models, and was endothermic and entropy-driven, with the spontaneity increasing with temperature. Volcanic rock@FeOOH displayed strong binding affinity for NH_4^+-N under neutral and alkaline conditions, and retained considerable NH_4^+-N adsorption capacity even in the presence of coexisting cations. The main adsorption mechanism involves a combination of electrostatic interaction and coordination bonding. Moreover, the saturated material exhibited minimal desorption in water and alkaline solutions, and a low cumulative nitrogen release rate (1.4%) in soil leaching experiments versus unmodified rock (4.2%), indicating its potential as a slow-release fertilizer. Overall, volcanic rock@FeOOH is a promising material for the capture, recovery, and agricultural reuse of NH_4^+-N from wastewater.

Keywords: ammonia nitrogen; adsorption; volcanic rock; hydroxyl iron oxide; application potential

Check for updates

Academic Editor: Laura Bulgariu

Received: 31 October 2026
Revised: 16 November 2026
Accepted: 18 November 2026
Published: 21 November 2026

Copyright: © 2026 by the authors. Licensee MDPI, Basel, Switzerland. This article is an open access article distributed under the terms and conditions of the Creative Commons Attribution (CC BY) license.

1. Introduction

The excessive discharge of ammonia nitrogen is a key driver of aquatic eutrophication [1]. Various methods have been developed for ammonia nitrogen removal from wastewater, which can be broadly categorized into two groups according to their primary objectives: disposal-oriented approaches and resource-recovery-oriented approaches. Disposal-oriented methods, such as biological treatment [2] and breakpoint chlorination [3], focus on the complete elimination of ammonia nitrogen from wastewater. In contrast, resource-recovery-oriented methods, including chemical precipitation [4], air stripping [5], membrane separation [6], and adsorption [7], aim to simultaneously remove and recover ammonia nitrogen in valuable forms. From the perspective of the circular economy, the latter strategies are more attractive as they promote nitrogen resource recycling and reduce environmental pollution.

Among resource-recovery-oriented techniques, adsorption is favored for its simplicity of operation, high efficiency, and good cost-effectiveness. Specifically, soil amendments—such as biochar, volcanic rocks, clay minerals, and zeolites—have been widely used in agriculture. These materials can not only be used for ammonia nitrogen adsorption from wastewater, but the spent adsorbents can also be directly applied to soil, helping improve soil aeration and drainage, conserve fertilizer, and increase crop yield. This enables the utilization of spent adsorbents as slow-release fertilizers and promotes sustainable nitrogen fertilizer management. Meanwhile, it also avoids the regeneration and disposal issues associated with conventional adsorbents.

Based on this concept, several studies have been conducted. Zhou et al. [8] synthesized a sodium-acetate-modified synthetic zeolite (MSZ) for ammonium adsorption from simulated wastewater; when applied to mung bean cultivation, the ammonium-loaded MSZ significantly promoted seed germination and plant growth. Faccini et al. [9] applied zeolitite enriched with NH_4^+ via pig slurry in a 3-year field trial, demonstrating that it effectively reduced NO_3^- leaching and maintained crop yields despite a reduction in chemical nitrogen fertilizer input. Shao et al. [10] fabricated modified ceramsite from sewage sludge and fly ash to recover nitrogen and phosphorus from real wastewater treatment plant effluent, and subsequently used the N&P-adsorbed ceramsite as a slow-release fertilizer to promote the germination, growth, and blooming of *Impatiens commelinoides*. Sun et al. [11] prepared a nitrogen-loaded sulfonic-humic acid char (SHAC) from weathered coal humic acid; the SHAC exhibited slower nutrient release kinetics than commercial ammonium chloride and improved wheat yield while increasing residual NH_4^+-N in the soil. Furthermore, Zhao et al. [12] prepared modified biochar (RM/RSBC) from red mud and rape straw to effectively recover nitrogen and phosphorus from phosphorus mine wastewater, and the nutrient-loaded biochar significantly promoted mung bean growth when applied as a soil amendment.

The above cases confirm the viability of using soil amendments for ammonia nitrogen recovery and agricultural reuse; however, unmodified raw materials inherently exhibit weak adsorption capacity. This limitation stems from the simple pore structures of natural minerals and the lack of abundant active functional groups in biochar, resulting in poor binding affinity for NH_3/NH_4^+. To overcome this drawback for practical applications, modification strategies are essential. These modification methods can be roughly divided into two categories: physical modification, including sonication, calcination (to increase surface area), and pelletization (to avoid pressure drop); and chemical modification, such as acid/base treatment, oxidation, and coating, which aim to promote binding affinity [7]. Targeted chemical modification has been validated as effective in enhancing ammonia nitrogen adsorption on soil amendments. For example, Feng et al. [13], Shi et al. [14], and Zhou et al. [15] significantly improved the ammonia nitrogen adsorption capacities of natural kaolin, steel slag, and tailings containing layered silicate minerals by modifying them with NaOH, $MgCl_2$, and manganese oxide, respectively.

Among various soil amendments, volcanic rock has attracted particular attention for its dual functionality as a widely used soil amendment in agriculture and a commonly used matrix material in water treatment [16]. However, its natural micrometer- or millimeter-scale pores and low specific surface area severely limit its ammonia nitrogen adsorption capacity [17]. To address this shortcoming, hydroxyl iron oxide (FeOOH) presents a promising modifier: it offers a high specific surface area, abundant binding sites, and stable chemical properties, with its surface charge and amphoteric functional groups promoting ammonia nitrogen adsorption [18]. Since bare FeOOH nanoparticles are prone to loss due to their fine size, loading them onto volcanic rock can synergistically resolve the structural limitations of the rock and the separation issues of the iron oxide. Theoretically, this

composite strategy is expected to significantly enhance ammonia nitrogen capture. The feasibility of such a loading concept has been corroborated by Xu et al. [19], who successfully loaded iron oxide nanoparticles onto zeolite for efficient nutrient removal.

However, studies on FeOOH-modified volcanic rock that systematically investigate its adsorption mechanisms and evaluate the potential of spent adsorbents as slow-release fertilizers remain scarce. In this context, this study aims to develop a FeOOH-modified volcanic rock composite (volcanic rock@FeOOH) via co-precipitation, systematically investigate its NH_4^+-N adsorption behavior and mechanisms, and further evaluate the application potential of NH_4^+-N-saturated composite as a slow-release fertilizer. This would provide a sustainable pathway for nitrogen resource recovery from wastewater.

2. Materials and Methods

2.1. Preparation of Sample

2.1.1. Pretreatment of Volcanic Rock

The volcanic rock used in this study was purchased from Tianjin Yaxin Weiye Mineral Products Sales Department in Tianjin, China. The raw material was repeatedly washed with deionized water and dried to constant weight in an electric thermostatic drying oven. The dried rock was ground in a ceramic mortar and sifted through 10-mesh-to-18-mesh sieves to obtain volcanic rock particles measuring 1–2 mm. The sieved particles were then washed again 2–3 times with deionized water and dried to constant weight in the drying oven for future use.

2.1.2. Preparation of Volcanic rock@FeOOH

The volcanic rock@FeOOH composite was prepared via a co-precipitation method. The pretreated volcanic rock was first activated by soaking in a 0.5 mol·L^{-1} NaCl solution for 4 h, then washed with 20% anhydrous ethanol and deionized water, and dried at 60 °C to constant weight. After that, the activated volcanic rock was immersed in a mixed solution containing saturated NaCl, 0.5 mol·L^{-1} $FeCl_3 \cdot 6H_2O$, and 20% (v/v) ethanol aqueous solution. A 1.5 mol·L^{-1} NaOH solution was added dropwise to adjust the pH to 2.8, and the mixture was oscillated in a thermostatic shaker at 25 °C for 12 h. After the reaction was completed, the product was filtered and washed sequentially with a 2 mol·L^{-1} NaCl solution and a 30% (v/v) ethanol aqueous solution. Finally, the sample was heat treated in a 105 °C vacuum drying oven for 12 h to obtain the volcanic rock@FeOOH composite.

2.2. Sample Characterization

The crystal structure of the prepared samples was analyzed by X-ray diffraction (XRD) on a Bruker D8 Advance diffractometer (Bruker AXS GmbH, Karlsruhe, Germany) using Cu Kα radiation (λ = 1.5406 Å) at 40 kV and 40 mA, with a scanning step of 5°·min^{-1} over a 2θ range of 5–90°. Surface morphology was observed using a Quanta FEG 450 scanning electron microscope (SEM, FEI Company, Hillsboro, OR, USA) at an accelerating voltage of 15 kV. Specific surface area was calculated using the Brunauer–Emmett–Teller (BET) method, and pore size distribution were determined via N_2 adsorption–desorption at −196 °C using a Kubo-X1000 surface area and porosity analyzer (Beode Electronic Technology Co., Ltd., Beijing, China). Prior to analysis, the sample was degassed at 200 °C for 5 h to remove physically adsorbed impurities. Fourier-transform infrared (FTIR) spectra were recorded on a NICOLET IS20 spectrometer (Thermo Fisher Scientific Inc., Waltham, MA, USA) over the range of 3500–400 cm^{-1}. Surface chemical composition and elemental valence states were examined using a K-Alpha X-ray photoelectron spectrometer (XPS, Thermo Fisher Scientific Inc., Waltham, MA, USA) with monochromatic Al Kα (1486.6 eV) radiation, and the binding

energies were calibrated against the C 1s peak at 284.8 eV. Zeta potential measurements were performed using a Zeta potential analyzer (SZ-100Z, HORIBA, Ltd., Kyoto, Japan) over a pH range of 3.0–12.0.

2.3. Adsorption Experiments

Batch adsorption experiments were conducted to evaluate the ammonia nitrogen adsorption performance of natural volcanic rock and volcanic rock@FeOOH. In this study, the adsorption performance was compared between pristine volcanic rock and volcanic rock@FeOOH, because bare FeOOH is prone to particle loss and is not intended for direct use as an adsorbent in soil or column applications. Unless otherwise specified, each experiment was performed by adding 0.5 g of adsorbent to 250 mL of NH_4^+-N solution in a 500 mL conical flask with a ground-glass stopper and shaking at 150 r·min^{-1} in a thermostatic shaker until equilibrium was reached. This dose was selected based on preliminary dose experiments (0.5–8 g·L^{-1}), in which the unit adsorption capacity decreased with increasing dose while the removal efficiency increased; 2 g·L^{-1} provided a reasonable balance between NH_4^+-N removal and adsorbent utilization. The corresponding dose-dependent adsorption capacity and removal efficiency are provided in Supplementary Figure S1. All NH_4^+-N solutions were prepared by dissolving NH_4Cl in deionized water. The residual NH_4^+-N concentration was determined using Nessler's reagent spectrophotometry (HJ 535-2009). The calculation method for the adsorption capacity of adsorbent is as follows:

$$q_t = \frac{(C_0 - C_t)V}{W} \quad (1)$$

where q_t (mg·g^{-1}) is the adsorption capacity at time t (min); C_0 (mg·L^{-1}) is the initial NH_4^+-N concentration; C_t is the NH_4^+-N concentration at time t (mg·L^{-1}); V (L) is the total volume of ammonia nitrogen solution; and W (g) is the adsorbent dosage. All experiments were conducted in triplicate, and the average values were reported.

2.3.1. Adsorption Kinetics

Adsorption kinetics were investigated at 25 °C with an initial NH_4^+-N concentration of 10 mg·L^{-1}. Samples were collected at predetermined time intervals to determine the residual NH_4^+-N concentration. The kinetic data were fitted using pseudo-first-order and pseudo-second-order models. The fitting formulas are as follows:

$$\text{Pseudo-first-order kinetic equation } \ln(q_e - q_t) = \ln q_e - k_1 t \quad (2)$$

$$\text{Pseudo-second-order kinetic equation } \frac{t}{q_t} = \frac{1}{k_2 q_e^2} + \frac{t}{q_e} \quad (3)$$

where q_e (mg·g^{-1}) is the equilibrium adsorption capacity; k_1 (min^{-1}) and k_2 (g·mg^{-1}·min^{-1}) are the pseudo-first-order and pseudo-second-order rate constants, respectively.

2.3.2. Adsorption Isotherms

Adsorption isotherms were determined at 25 °C using initial NH_4^+-N concentrations ranging from 5 to 150 mg·L^{-1}. The equilibrium data were fitted using the Langmuir and Freundlich models. The formulas are as follows:

$$\text{Langmuir equation } \frac{1}{q_e} = \frac{1}{K_L q_m C_e} + \frac{1}{q_m} \quad (4)$$

$$\text{Freundlich equation } \ln q_e = \ln K_f + \frac{1}{n} \ln C_e \quad (5)$$

where q_m (mg·g^{-1}) is the maximum monolayer adsorption capacity; K_L (L·mg^{-1}) is the Langmuir constant; C_e (mg·L^{-1}) is the equilibrium concentration; K_f (L·mg^{-1}) is the Freundlich constant; and n is the heterogeneity factor.

2.3.3. Adsorption Thermodynamics

Thermodynamic parameters were evaluated at 15, 25, and 35 °C with an initial NH_4^+-N concentration of 10 mg·L^{-1}. The parameters were calculated using the following thermodynamic formulas [20]:

$$\Delta G = \Delta H - T\Delta S \quad (6)$$

$$\Delta G = -RT \ln K_e \quad (7)$$

$$\ln K_e = -\frac{\Delta H}{RT} + \frac{\Delta S}{R} \quad (8)$$

where ΔG (kJ·mol^{-1}) is the Gibbs free energy change; ΔH (kJ·mol^{-1}) is the enthalpy change; ΔS (kJ·mol^{-1}·K^{-1}) is the entropy change; R is the universal gas constant (8.314 J·mol^{-1}·K^{-1}); T (K) is the absolute temperature; and K_e is the thermodynamic equilibrium constant.

2.3.4. Investigation of Influencing Factors

The effects of initial pH (3.0–12.0) and coexisting cations on NH_4^+-N adsorption were investigated at 25 °C, with an initial NH_4^+-N concentration of 10 mg·L^{-1}. The effects of coexisting cations (Na^+, K^+, and Mg^{2+}) on NH_4^+-N adsorption were investigated under neutral conditions. Both single-ion systems (individual addition of Na^+, K^+, or Mg^{2+}) and mixed-ion systems (simultaneous addition of all three cations) were examined at concentrations of 0.01, 0.1, and 1.0 mol·L^{-1}. Both the pH and coexisting-cation adsorption experiments were conducted with a contact time of 120 min, after which the residual NH_4^+-N concentrations were measured for each condition. Adsorbent-free control experiments at pH 3.0, 5.0, 7.0, 10.0, and 12.0 under identical shaking conditions showed that the NH_4^+-N loss was less than 5% after 120 min; therefore, no blank correction was applied.

2.4. Evaluation of the Application Potential

2.4.1. Desorption Experiments

Fresh adsorbent (0.5 g) was added to 250 mL of NH_4^+-N solution with an initial concentration of 10 mg·L^{-1} in a 500 mL conical flask with a ground-glass stopper. The pH was adjusted to 7.0, and the mixture was shaken at 25 °C and 150 r·min^{-1} for 24 h to allow adsorption. After adsorption, the adsorbent was filtered and air-dried to obtain the NH_4^+-N saturated adsorbent. The adsorption capacity was calculated according to Equation (1) in Section 2.3. The saturated adsorbent was then placed into 250 mL of deionized water, NaOH solution (0.5 mol·L^{-1}), and HCl solution (0.5 mol·L^{-1}), respectively, with a dosage of 0.5 g in each 250 mL of desorption solution. The mixtures were shaken at 25 °C and 150 r·min^{-1} for 2160 min to reach desorption equilibrium. Samples were taken at specific time intervals to measure the NH_4^+-N concentration. The desorption capacity at each sampling time was calculated as follows:

$$q_{d,t} = \frac{C_{d,t}V}{W} \quad (9)$$

where $q_{d,t}$ (mg·g^{-1}) is the desorption capacity at time t and $C_{d,t}$ (mg·L^{-1}) is the NH_4^+-N concentration in the desorption solution at time t.

2.4.2. Soil Column Leaching Experiment

To evaluate the nitrogen leaching risk after the application of the NH_4^+-N-saturated adsorbent to soil, a soil column leaching experiment was conducted (the experimental device is shown in Supplementary Figure S2). The total water input was designed based on the average annual rainfall in Guilin, Guangxi, China, which was 2217.21 mm over the period 2022–2024. The estimated total water input was approximately 8.70 L for a two-year rainfall simulation, which was rounded to 9 L for experimental convenience.

The test soil was mixed with the NH_4^+-N-saturated adsorbent and packed into leaching columns (5 cm in diameter, 20 cm in height), with a column containing only soil serving as the control. Before the first leaching event, each column was pre-wetted with 250 mL of deionized water and allowed to stand for 24 h. Thereafter, a total of 9 leaching events (1 L each) were conducted at 1-day intervals (with the first leaching event occurring on day 1). The leachate was collected for NH_4^+-N concentration determination. Each treatment was performed in triplicate. Detailed experimental parameters and procedures are provided in Supplementary Section S2.

The cumulative release rate (R_{cum}, %) after a given number (n) of leaching events was calculated as:

$$R_{cum} = \frac{\sum_{i=1}^{n} C_i \times V_i}{q \times W} \times 100\% \quad (10)$$

where q (mg·g^{-1}) is the adsorption capacity of the adsorbent, W (g) is the mass of adsorbent packed in the column, C_i (mg·L^{-1}) is the NH_4^+-N concentration in the leachate of the i-th leaching event, and V_i (L) is the volume of leachate collected in the i-th leaching event. In this study, V_i was approaching 1 L per event.

3. Results and Discussion

3.1. Structure and Surface Properties of the Materials

3.1.1. Morphology and Structure Characteristics

The XRD patterns of volcanic rock and volcanic rock@FeOOH are shown in Figure 1a. Both samples exhibit the strongest diffraction peak at 2θ = 26.6°, corresponding to the (101) plane of SiO_2. Other relatively strong diffraction peaks appear at 2θ = 22.6–22.7°, 29.6–29.8°, and 35.2–35.5°, which are assigned to the Al_2O_3, Ca_2SiO_4, and overlapping Ca-containing phases (e.g., CaO/Ca_2SiO_4), respectively. Compared with pristine volcanic rock, volcanic rock@FeOOH shows additional diffraction peaks at 2θ = 26.8°, 34.1°, 35.3°, 39.2°, 46.5°, 52.0°, and 56.0°. Some of these positions coincide with β-FeOOH (PDF 34-1266) [21], but they overlap with the diffraction peaks of the volcanic rock matrix. The characteristic low-angle β-FeOOH peaks at 11.8° and 16.7° were not clearly observed, likely due to the low loading amount and/or low crystallinity of FeOOH. Therefore, XRD provides supporting evidence for FeOOH loading, and the successful loading is further confirmed by FTIR, XPS, SEM, and BET results.

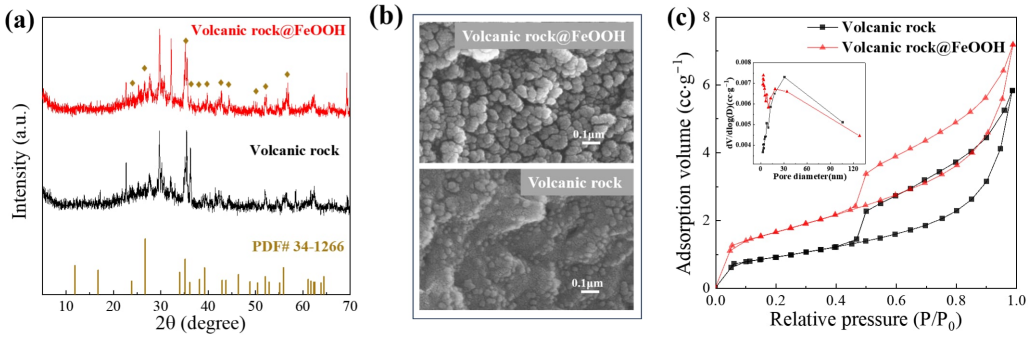


Figure 1. (**a**) XRD patterns, (**b**) SEM images, and (**c**) N_2 adsorption–desorption isotherms and pore size distribution (inset) of volcanic rock and volcanic rock@FeOOH.

From the SEM images (Figure 1b), it can be observed that compared to volcanic rock, the surface of volcanic rock@FeOOH is covered with cluster-like particles and exhibits obvious pores. The N_2 adsorption–desorption results are shown in Figure 1c and Table 1. The adsorption isotherms of volcanic rock samples before and after modification are both typical type IV with an H4 hysteresis loop, indicating that the pores of this type of material

are primarily a combination of micropores and mesopores. After modification, the specific surface area (SBET) of volcanic rock@FeOOH increased by 1.79 times relative to that of natural volcanic rock, accompanied by increases in total pore volume (V_t) and micropore volume (V_{mi}), while the average pore size decreased. This indicates that the loaded FeOOH particles created abundant micropores between the surface clusters, thereby enhancing specific surface area and pore volume. Meanwhile, the reduced pore width suggests that FeOOH might have infiltrated into the internal fissures and pores, implying that the active sites of FeOOH also exist within the pore channels. These textural changes increase the accessibility of surface active sites, which is beneficial for adsorption.

Table 1. Specific surface area and pore structure parameters of volcanic rock and volcanic rock@FeOOH obtained from N_2 adsorption–desorption analysis.

Materials	SBET ($m^2 \cdot g^{-1}$)	Vt ($cm^3 \cdot g^{-1}$)	Vmi ($cm^3 \cdot g^{-1}$)	Average Pore Size (nm)
Volcanic rock	3.2512	0.0090	0.001376	5.54
Volcanic rock@FeOOH	5.8130	0.0111	0.002494	3.82

3.1.2. Chemical Structure Characteristics

The FTIR spectra of volcanic rock and volcanic rock@FeOOH are shown in Figure 2a. Both samples exhibit common absorption peaks: a broad absorption peak between 3500~3400 cm^{-1}, corresponding to the O-H stretching vibration of intermolecular hydrogen bonding [22]; a saturated C-H stretching vibration at 3000 ~ 2700 cm^{-1} [22]; a C=O double bond at 1650~1400 cm^{-1} [22]; a Si-O-Si (Al) stretching vibration peak at 1100~1000 cm^{-1} [23]; and an absorption band at approximately 453 cm^{-1}, which can be attributed to the Si–O bending vibrations of the volcanic rock matrix [22,24], with a possible overlapping contribution from Fe–O vibrations [25]. Through comparison, it can be found that the modified volcanic rock@FeOOH exhibits new characteristic peaks between 900 and 420 cm^{-1}, which can be attributed to the out-of-plane bending vibration of Fe-hydroxy groups in the β-FeOOH crystal structure [26]. The results show that the volcanic rock@FeOOH was synthesized successfully, which is consistent with the aforementioned XRD results. The Fe–OH groups within FeOOH have been reported to serve as effective adsorption sites for pollutants [27]. Additionally, theoretically, the mobile π-electrons in the C=O double bond can be drawn towards to more electronegative oxygen atoms, increasing the polarity between carbon and oxygen, thereby making it easier for C=O to attract positively charged ions. It can be inferred that the presence of FeOOH and the C=O double bond in volcanic rock@FeOOH may contribute to its enhanced NH_4^+-N adsorption capacity.

Figure 2b shows the XPS full spectra of volcanic rock and volcanic rock@FeOOH. Peaks corresponding to Na 1s, Fe 2p, O 1s, N 1s, C 1s, Si 2p, and Al 2p can be observed in both samples. The corresponding elemental content data is summarized in Table S1. Notably, the relative Fe content in volcanic rock@FeOOH decreased compared with that of pristine volcanic rock, which may be attributed to the partial dissolution of iron from the volcanic rock under the acidic conditions (pH 2.8) during the co-precipitation process. It should be noted that XPS probes only the near-surface region and reports relative atomic percentages rather than total Fe content; therefore, the lower surface Fe percentage does not contradict the successful loading of FeOOH, which is supported by Fe–OH/Fe–O infrared bands, surface cluster morphology, increased specific surface area, and micropore volume, together with the supporting XRD evidence after accounting for peak overlap with the volcanic rock matrix. Additionally, the sodium content in volcanic rock@FeOOH increasd. This is because

the small amount of NaCl used in the activation process was not washed, and remained on the material.

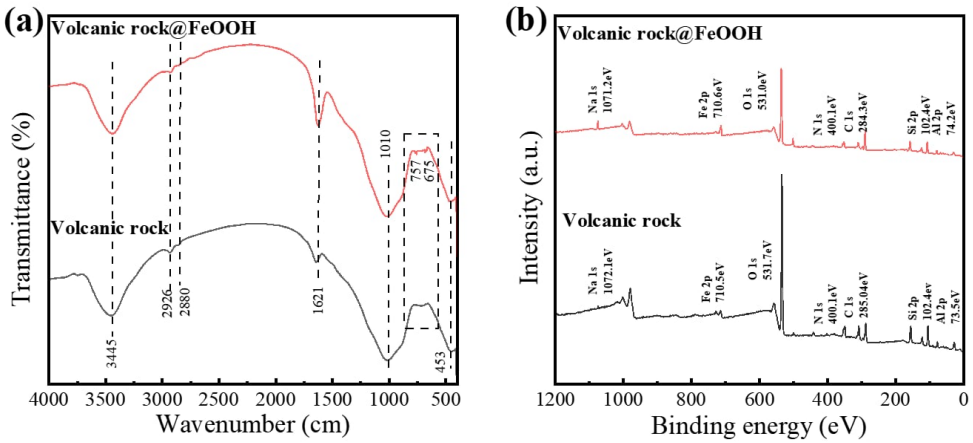


Figure 2. (**a**) FTIR and (**b**) XPS spectra of volcanic rock and volcanic rock@FeOOH.

Figure 3a shows the Fe 2p deconvoluted spectra. The high-resolution Fe 2p peaks are asymmetric, indicating the presence of more than one oxidation state of iron. The binding energies of the peaks correspond to Fe^{2+} and Fe^{3+}. For Fe 2p, each oxidation state peak consists of two spin-orbit coupling peaks (Fe $2p_{1/2}$ and Fe $2p_{3/2}$). The fitting parameters show a binding energy difference of $\Delta E_b = E_b$ (Fe $2p_{1/2}$) − E_b (Fe $2p_{3/2}$) = 13.1 eV, with a peak area ratio of 0.5. Using Fe $2p_{3/2}$ as a representative, the percentage content of Fe^{3+} and Fe^{2+} are summarized in Table S2. It can be found that the relative content of Fe^{3+} in volcanic rock@FeOOH increased by approximately 13.5% after loading FeOOH. As we know, Fe^{3+} has more electron vacancies than Fe^{2+}. The increase in electron vacancies can enhance the possibility of forming coordination bonds by attracting electron pairs, and it is possible to attract electrons to carry negative charges, thereby enhancing the electrostatic attraction with positively charged cations [28].

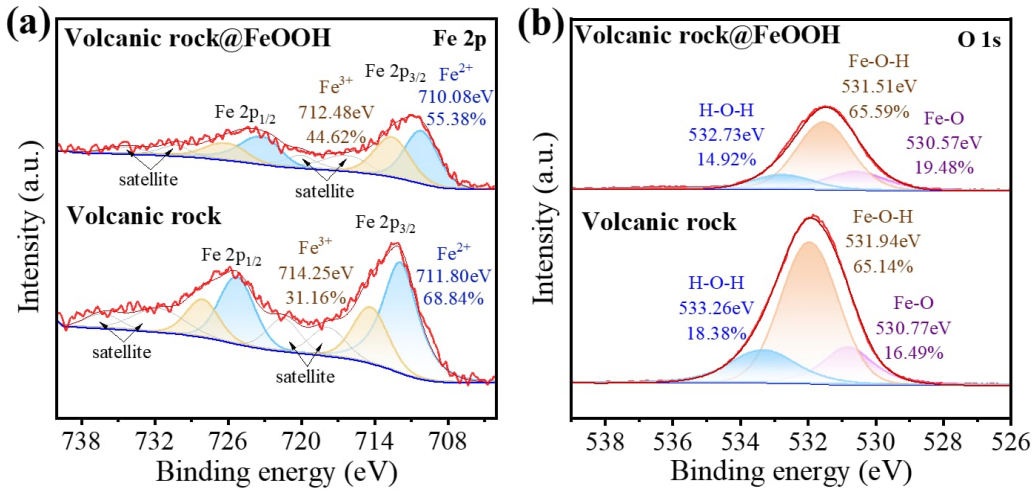


Figure 3. (**a**) Fe 2p and (**b**) O 1s spectra of volcanic rock and volcanic rock@FeOOH.

Figure 3b shows the O 1s deconvoluted spectra. In order of binding energy from high to low, the sub-peaks located at 532.7 eV, 531.5 eV, and 530.6 eV correspond to oxygen in water molecules (H-O-H), hydroxyl oxygen bonded to metals (Fe-O-H), and lattice oxygen bonded to metals (Fe-O), respectively. As can be seen from Figure 3b and Table S2, the relative content of Fe-O increased from 16.49% to 19.48% after modification, while Fe-O-H remained nearly unchanged (65.14% vs. 65.59%). The hydroxyl oxygen can combine with

adsorbates to form hydrogen bonds and coordination bonds, while the oxygen atoms in lattice oxygen are negatively charged and easily attract positively charged cations [29]. Therefore, theoretically, the increase in hydroxyl oxygen and lattice oxygen could help to enhance the adsorption capacity of materials.

3.2. Ammonia Nitrogen Adsorption Performance by Volcanic rock@FeOOH

3.2.1. Adsorption Kinetics

The fitting results of the adsorption models of volcanic rock and volcanic rock@FeOOH are shown in Figure 4a and Table 2. The R^2 of pseudo-second-order kinetic model were higher than those for the pseudo-first-order model, suggesting that the adsorption process conforms more to the kinetics of a second-order reaction. The second-order reaction kinetic model is particularly suitable for describing the diffusion of adsorbate from solution to the surface of the adsorbent when the adsorption process is controlled by a chemisorption mechanism [30]. Thus, it suggests that the adsorption of NH_4^+-N onto volcanic rock@FeOOH may involve surface-site-dependent processes, such as electrostatic interaction and coordination with FeOOH functional groups. In addition, the k_2 of volcanic rock@FeOOH is less than that of volcanic rock, indicating that the adsorption process on the modified material was relatively slower, which may be attributed to the involvement of additional surface interactions and diffusion within the modified porous structure. Nevertheless, the equilibrium adsorption capacity of volcanic rock@FeOOH (3.690 $mg \cdot g^{-1}$) was significantly higher than that of volcanic rock (1.817 $mg \cdot g^{-1}$), indicating that FeOOH loading effectively increased the number of active adsorption sites and improved the overall NH_4^+-N uptake.

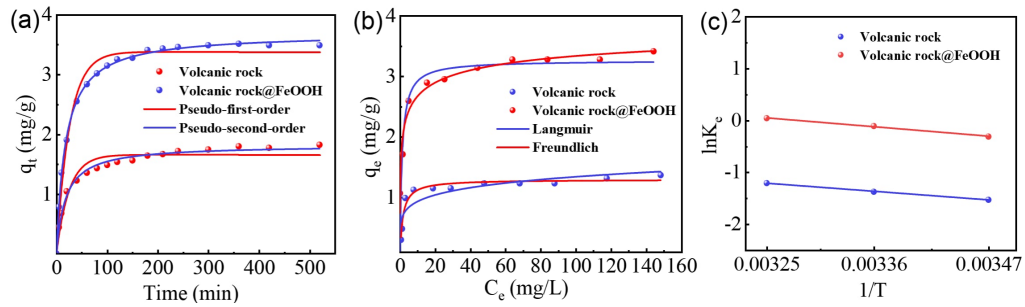


Figure 4. (**a**) Adsorption kinetics, (**b**) adsorption isotherms, and (**c**) adsorption thermodynamics of volcanic rock and volcanic rock@FeOOH.

Table 2. Adsorption kinetics model parameters of volcanic rock and volcanic rock@FeOOH.

Dynamic Model		Volcanic Rock	Volcanic rock@FeOOH
Pseudo-first-order model	k_1	0.040	0.039
	q_e ($mg \cdot g^{-1}$)	1.655	3.378
	R^2	0.946	0.982
Pseudo-second-order model	k_2	0.031	0.015
	q_e ($mg \cdot g^{-1}$)	1.817	3.690
	R^2	0.991	0.999

3.2.2. Isothermal Adsorption Performance

The fitting results of adsorption isotherms of volcanic rock and volcanic rock@FeOOH are shown in Figure 4b and Table 3. Under identical conditions, the adsorption capacity of volcanic rock@FeOOH for NH_4^+-N was significantly higher than that of volcanic rock. This enhancement can be attributed to the increased specific surface area and the resulting better exposure of adsorption active sites of volcanic rock after FeOOH loading. Notably,

the adsorption data of pristine volcanic rock were better described by the Langmuir model, suggesting that NH_4^+-N adsorption on the unmodified material predominantly followed monolayer adsorption [7]. In contrast, the adsorption data of volcanic rock@FeOOH were better fitted by the Freundlich model, indicating that the heterogeneity characteristics have been enhanced after modification. This suggests that the adsorption of NH_4^+-N onto volcanic rock@FeOOH likely involves multiple mechanisms.

Table 3. Adsorption isotherm model parameters of volcanic rock and volcanic rock@FeOOH.

Isothermal Adsorption Model		Volcanic Rock	Volcanic rock@FeOOH
Langmuir	K_L ($L \cdot mg^{-1}$)	0.640	0.852
	q_m ($mg \cdot g^{-1}$)	1.290	3.260
	R^2	0.952	0.867
Freundlich	K_f ($L \cdot mg^{-1}$)	0.643	1.833
	n	6.301	4.873
	R^2	0.764	0.969

3.2.3. Adsorption Thermodynamics

The linear fit of lnKe versus $1/T$ for volcanic rock and volcanic rock@FeOOH is shown in Figure 4c, and the corresponding thermodynamic parameters (ΔH, ΔS, and ΔG) at different temperatures are summarized in Table 4. The values of ΔH and ΔS are both greater than 0. This indicates that the adsorption process was an endothermic process, that the randomness or disorder of solid-solution interface increased during adsorption [31], and that increasing temperature was conducive to the spontaneous process of adsorption. Given the stoppered flasks and the small control loss (<5%), this apparent endothermicity is unlikely to be dominated by NH_3 volatilization. In addition, it is reported that the heats of physical adsorption are of the same order of magnitude as the heat of condensation, 2.1 to 20.9 $kJ \cdot mol^{-1}$, while the heats of chemisorption generally change from 80 to 200 $kJ \cdot mol^{-1}$ [32]. The ΔH values of the adsorption reaction in this study both fall within the physical adsorption range, suggesting that physical adsorption is the dominant contribution to NH_4^+-N uptake by both adsorbents. The slightly higher ΔH of volcanic rock@FeOOH than that of volcanic rock indicates a somewhat stronger adsorption interaction after FeOOH loading, while its larger ΔS indicates a stronger entropy driving force. Notably, the ΔG values of volcanic rock@FeOOH decreased markedly with increasing temperature and became negative at 308 K, indicating that FeOOH loading improved the spontaneity of the adsorption reaction. In contrast, the ΔG values of pristine volcanic rock remained positive over the tested temperature range. Combined with the kinetic and isotherm results, the relatively low ΔH values suggest that physical adsorption may contribute substantially to NH_4^+-N uptake, while the better fit of the pseudo-second-order kinetic model and the Freundlich isotherm indicates that surface-site-dependent interactions, such as electrostatic interaction and coordination bonding, may also be involved in the adsorption process on volcanic rock@FeOOH.

Table 4. Thermodynamic parameters for the adsorption of ammonia nitrogen by volcanic rock and volcanic rock@FeOOH.

Materials	T (K)	ΔH (kJ·mol^{-1})	ΔS (J·mol^{-1}·K^{-1})	ΔG (kJ·mol^{-1})	R^2
Volcanic rock	288	11.872	28.456	3.667	0.998
	298			3.412	
	308			3.097	
Volcanic rock @FeOOH	288	13.016	42.656	0.747	0.995
	298			0.270	
	308			−0.104	

3.2.4. Effect of pH on NH_4^+-N Adsorption

The adsorption capacities of volcanic rock and volcanic rock@FeOOH for ammonia nitrogen under different pH conditions are shown in Figure 5a. The maximum capacity for absorption occurs under neutral conditions. In acidic conditions, the adsorption capacity decreases with increasing acidity, while in alkaline conditions, the capacity remains relatively stable with changes in pH. The difference in NH_4^+-N adsorption capacity in different pH ranges may be related to the changes in the existing forms of ammonia nitrogen in the solution [33]. The equilibrium reaction of ammonia nitrogen in solution is as follows:

$$NH_3 + H_2O \rightleftharpoons NH_4^+ + OH^- \quad (11)$$

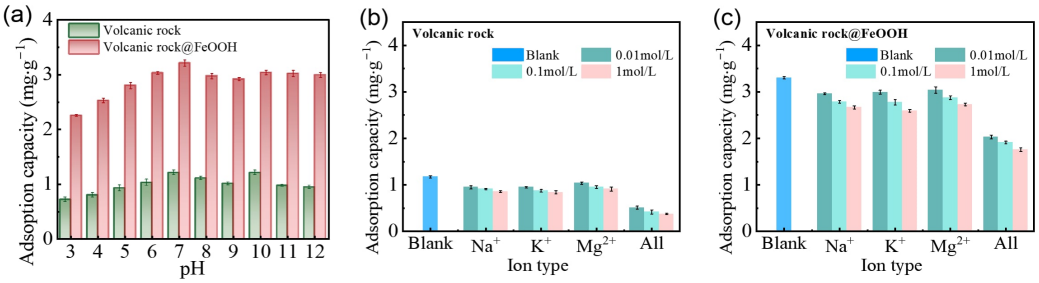


Figure 5. Effects of (**a**) pH and (**b**,**c**) coexisting ions on the adsorption of NH_4^+-N by volcanic rock and volcanic rock@FeOOH. (In the figure, "All" represent the cations (Na^+, K^+, Mg^{2+}) that were added as an equimolar mixture at the concentrations indicated in the legend.).

With the pK_a of NH_4^+ being approximately 9.25 at 25 °C, the solution pH governs the distribution of ammonia nitrogen between the ionic form (NH_4^+) and the molecular form (NH_3). At acidic-to-neutral pH, ammonia nitrogen predominantly exists as NH_4^+ ions. Under strongly acidic conditions, the abundant H^+ ions compete with NH_4^+ for adsorption sites on the material surface, thereby reducing the adsorption capacity [34]. As pH increases, the competitive effect of H^+ weakens, and the adsorption capacity rises, reaching its maximum under neutral conditions.

As pH further increases into the alkaline range, the proportion of NH_4^+ decreases while un-ionized NH_3 gradually becomes the dominant species. This reduces electrostatic attraction between the adsorbent and the adsorbate, which slightly lowers the adsorption capacity at pH 8–9 compared to the neutral condition. However, with the increasing abundance of NH_3, the overall variation in adsorption capacity across the alkaline pH range is not significant, suggesting that NH_3 molecules might bind to the adsorbent materials in a manner that did not occupy the adsorption sites for NH_4^+. Because the flasks were stoppered during shaking and the adsorbent-free control loss was less than 5% across the tested pH range, NH_3 volatilization did not dominate the pH-dependent adsorption trend.

3.2.5. Effect of Coexisting Cations on NH_4^+-N Adsorption

The effects of coexisting ions on the adsorption of ammonia nitrogen by volcanic rock and volcanic rock@FeOOH under neutral conditions are shown in Figure 5b,c. As the concentration of cations increases, the adsorption capacity of samples for ammonia nitrogen decreases, indicating that coexisting cations compete with ammonia nitrogen to some extent for adsorption. When Na^+, K^+, and Mg^{2+} coexist, their inhibition of the material's adsorption of NH_4^+-N is stronger than when each ion exists alone. Furthermore, even when the coexisting cation concentrations (0.01 mol·L^{-1}, 0.1 mol·L^{-1}, and 1 mol·L^{-1}) were higher than the NH_4^+-N concentration (0.000714 mol·L^{-1}), the materials still retained considerable NH_4^+-N adsorption capacity, indicating that the interference from coexisting cations was limited under the tested conditions.

3.3. Mechanism of Ammonia Nitrogen Adsorption by Volcanic rock@FeOOH

The adsorption mechanism of volcanic rock@FeOOH for ammonia nitrogen was investigated through a combination of morphological, structural, and spectroscopic analyses, and can be attributed to the synergistic effects of electrostatic interaction and coordination bonding.

Previous studies have demonstrated that electrostatic interaction is one of the dominant mechanisms for ammonia nitrogen adsorption [35]. As discussed in Section 3.1.2, Fe^{3+} and Fe^{2+} have the ability to attract electrons, acquiring a partial negative charge, while the oxygen atoms in Fe-O, C-O, and C=O are electronegative, facilitating positively charged NH_4+ cations. To verify its role in this system, zeta potential measurement of volcanic rock@FeOOH at different pH values was conducted. As shown in Figure 6a, the zeta potential of volcanic rock@FeOOH remains negative within the pH range of 3 to 12. This negative surface charge facilitates the electrostatic attraction of positively charged NH_4^+ ions, particularly under acidic to neutral conditions where NH_4^+ is the dominant species. The experimental results of the effect of pH and coexisting cations further support this mechanism. As discussed in Sections 3.2.4 and 3.2.5, the abundant H^+ ions and coexisting cations can compete with NH_4^+ for adsorption sites, leading to a decrease in adsorption capacity. These results collectively confirm that electrostatic attraction plays a major role in the adsorption process.

Furthermore, it is worth noting that the overall variation in adsorption capacity of volcanic rock@FeOOH across the alkaline pH range is not significant, suggesting that NH_3 molecules might bind to the adsorbent through mechanisms other than electrostatic interaction. According to previous reports, coordination adsorption and hydrogen bond adsorption are considered as possible pathways for NH_3 uptake [36], which may explain the sustained relatively high adsorption capacity under alkaline conditions, even when electrostatic attraction is no longer the dominant driving force.

Further evidence was provided by FTIR analyses and XPS analyses. As shown in Figure 6b, after NH_4^+-N adsorption, a new peak appears at 1349 cm^{-1} on the FTIR spectra of volcanic rock@FeOOH. This peak corresponds to the N-H bending vibration peak [33], confirming the effective adsorption of ammonia nitrogen by volcanic rock@FeOOH. Meanwhile, after adsorption, the peak position of the out-of-plane bending vibration absorption peak of Fe-O-H in the β-FeOOH crystal structure shifts from 757 cm^{-1} to 759 cm^{-1} and from 675 cm^{-1} to 673 cm^{-1}. These shifts indicate that Fe-O-H groups served as active adsorption sites of volcanic rock@FeOOH, and participated in the adsorption of ammonia nitrogen.

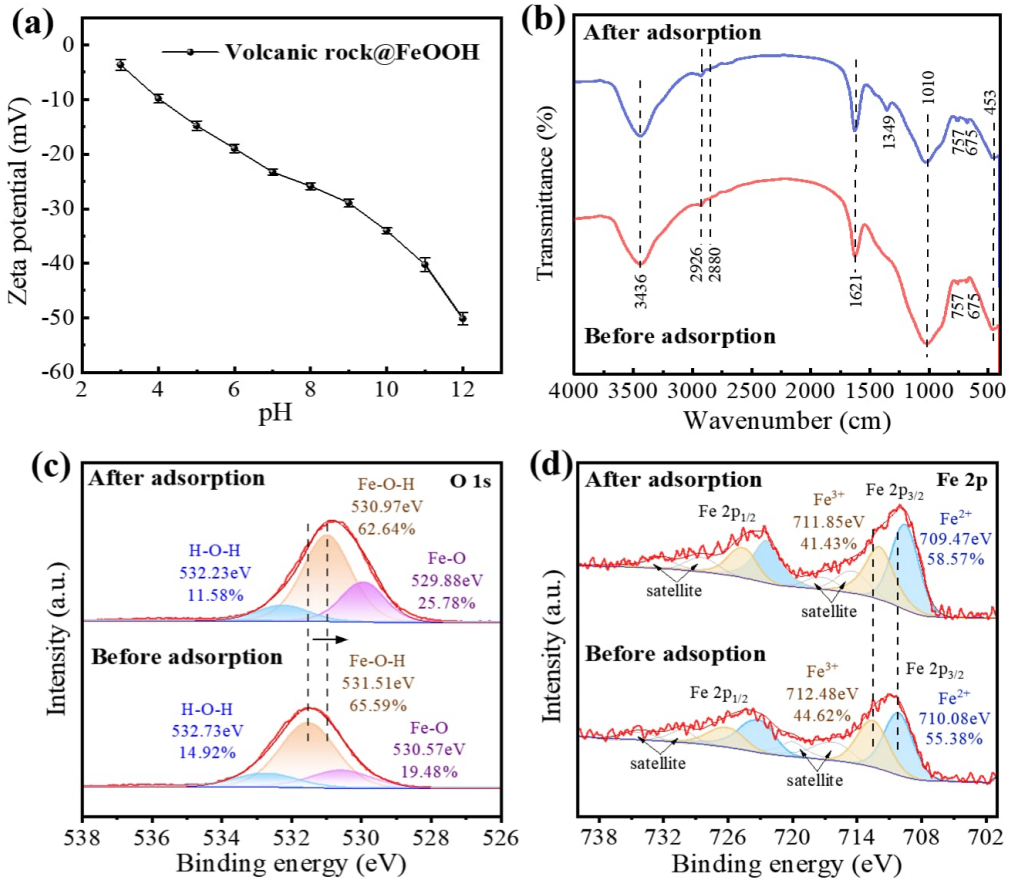


Figure 6. (**a**) Zeta potential of volcanic rock@FeOOH, (**b**) FTIR spectra of volcanic rock@FeOOH before and after adsorption, and (**c**,**d**) O 1s and Fe 2p spectra of volcanic rock@FeOOH before and after adsorption.

As shown in Figure 6c,d and Table S2, after NH_4^+-N adsorption, the binding energy of Fe-O-H shifts from 531.5 eV to 531.0 eV, and its relative content decreases from 65.6% to 62.6%. This suggests that the hydroxyl oxygen of Fe-O-H may coordinate with NH_3. Meanwhile, the binding energy of Fe^{3+} and Fe^{2+} shifts to lower values, and the relative contents of Fe^{3+} and Fe^{2+} also change. This indicates that the coordination environment of iron atoms is altered. Given that oxygen is more electronegative than nitrogen, the decreased binding energy likely reflects a transition from Fe–O to Fe–N bonds [37]. The above changes confirm the coordination between Fe sites and ammonia nitrogen. The possible coordination reactions are proposed as follows:

$$Fe^{3+} + 6NH_3 \rightarrow [Fe(NH_3)_6]^{3+} \quad (12)$$

$$Fe^{2+} + 2NH_3 \rightarrow [Fe(NH_3)_2]^{2+} \quad (13)$$

Besides electrostatic interaction and coordination bonding, other processes such as Fe leaching and ion exchange might also contribute to NH_4^+-N removal. Although these processes were not separately quantified in this study, the surface Fe and Na contents of volcanic rock@FeOOH changed only marginally after NH_4^+-N adsorption (Table S1), which is consistent with limited Fe dissolution and Na^+ release under the tested conditions. These processes are therefore considered unlikely to be the dominant contributors to NH_4^+-N uptake under the tested conditions, although a limited contribution from ion exchange cannot be completely excluded.

Overall, electrostatic interaction and coordination bonding are considered the primary adsorption mechanisms for NH_4^+-N. Owing to the combined effects of multiple mechanisms,

volcanic rock@FeOOH exhibits relatively stable adsorption performance across a wide pH range, particularly under neutral and alkaline conditions.

3.4. Application Potential of Materials

3.4.1. NH_4^+-N Desorption Performance in Different Desorption Solutions

The desorption performance of NH_4^+-N-saturated adsorbent in different desorption solutions is shown in Figure 7a,b and Table S3. In all cases, the desorption rate was relatively high only at the initial stage of the reaction, and remained slow throughout the rest of the reaction process. The desorption capacity of saturated adsorbent in different solutions follows the order HCl > NaOH > deionized water. Additionally, as detailed in Table S3, volcanic rock@FeOOH exhibited lower desorption percentages than volcanic rock under neutral and alkaline conditions, while its desorption rate was comparable to that of volcanic rock under acidic conditions. This indicates that the modified material possesses a stronger binding affinity for NH_4^+-N under neutral and alkaline conditions, whereas the beneficial effect of the modification is diminished in acidic environments.

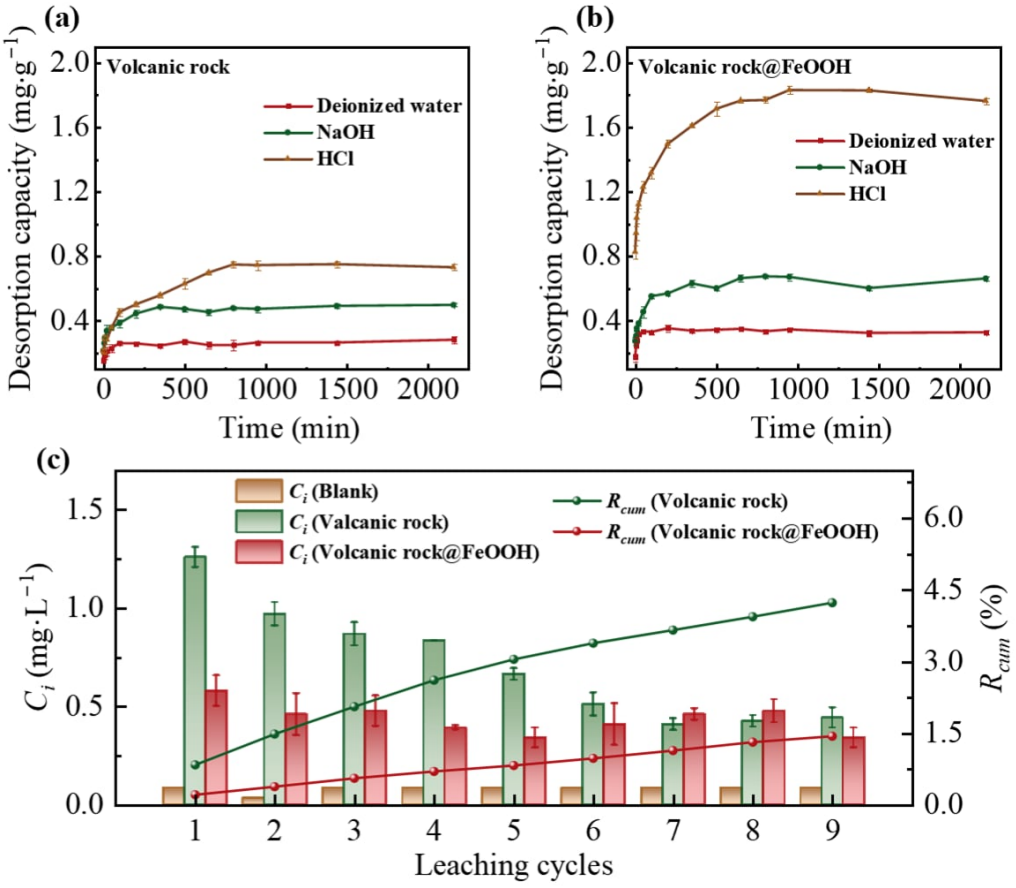


Figure 7. NH_4^+-N desorption from (**a**) volcanic rock and (**b**) volcanic rock@FeOOH under different desorption solutions, and (**c**) column leaching performance of volcanic rock and volcanic rock@FeOOH (1 L per leaching event, 24 h interval).

This difference in desorption performance can be attributed to the distinct mechanisms under each condition. In deionized water, the desorption of ammonia nitrogen is primarily driven by the dispersive effect of water molecules, which can release physically adsorbed NH_4^+ from the irregular surface of the adsorbent [38]. However, since the adsorption of ammonia nitrogen comprises the combined effects of physical adsorption and chemical adsorption, the desorption capacity of deionized water for ammonia nitrogen in adsorbents is limited. In alkaline conditions, the presence of OH^- in the solution generates electrostatic

effect with NH_4^+ in the adsorbent, causing it to desorb into the solution, resulting in an increased desorption rate compared to that in deionized water. In acidic solutions, the desorption efficiency is the highest among the three tested solutions. This can be attributed to two synergistic mechanisms: (1) H^+ ions compete with NH_4^+ for active adsorption sites and ion exchange sites, and (2) H^+ shifts the chemical equilibrium toward the ionic NH_4^+ form, facilitating their dissolution into the solution.

These results indirectly confirm that FeOOH loading enhances the binding affinity of the composite for NH_4^+-N, making it more effective at retaining ammonia nitrogen under neutral and alkaline conditions. The relatively low desorption efficiency in deionized water and alkaline solutions indicates that the material would resist nitrogen release under non-acidic soil conditions, supporting its potential as a slow-release fertilizer. However, the high desorption rates observed under acidic conditions (over 60%) indicate that the material's retention capacity is significantly weakened in acidic environments, and thus its application in acidic soils would require further evaluation.

3.4.2. NH_4^+-N Leaching Behavior in Soil Column Experiment

The results of the soil column leaching experiment are presented in Figure 7c. For the blank soil column (without any adsorbent), the NH_4^+-N concentration in the leachate remained consistently low throughout the entire leaching process, which is attributed to the combined effects of ammonia volatilization, nitrification, plant uptake, and runoff under natural conditions, resulting in a low background value of NH_4^+-N in the soil [39]. In contrast, the leachate from columns amended with NH_4^+-N-saturated adsorbents exhibited significantly higher NH_4^+-N concentrations than the blank control throughout the experiment.

In addition, there is a significant difference in the leaching patterns between unmodified volcanic rock and volcanic rock@FeOOH mixed soil columns. For the column containing saturated volcanic rock, the NH_4^+-N concentration in the leachate decreased sharply during the first 4 leaching events (corresponding to approximately one year of rainfall in Guilin). In the subsequent leaching events, the concentration remained relatively stable at a low level, indicating that most of the loosely bound ammonia nitrogen had been rapidly washed out. By contrast, the column containing saturated volcanic rock@FeOOH exhibited a relatively stable NH_4^+-N concentration in the leachate throughout the entire leaching process, without the sharp decline observed. This suggests that the FeOOH modification significantly enhanced the retention capacity of the adsorbent for ammonia nitrogen.

After nine leaching events, the cumulative release rate of NH_4^+-N from the column containing saturated volcanic rock was 4.2%, significantly higher than that from the column with saturated volcanic rock@FeOOH (1.4%). The relatively low cumulative release rates of both materials suggest their potential as slow-release nutrient carriers for agricultural application. Notably, FeOOH modification reduced the cumulative release rate by nearly 67% compared to unmodified volcanic rock, demonstrating its effectiveness in enhancing the slow-release performance of the adsorbent.

Overall, the soil column leaching results indicate that volcanic rock@FeOOH possesses superior slow-release performance compared to the unmodified volcanic rock. The enhanced retention and sustained release of ammonia nitrogen highlight its promising potential as a slow-release nitrogen fertilizer for agricultural applications, where nutrient losses via leaching can be effectively mitigated. It should be noted that salinity and metal release in the desorption and leaching solutions were not specifically quantified; however, given the washing procedure and the intended use as a soil amendment, these releases are expected to be limited and should be evaluated in future field-oriented studies.

4. Conclusions

In this study, volcanic rock@FeOOH was prepared by co-precipitation method and then used for the enrichment of ammonia nitrogen from aqueous solution. Characterization analyses revealed that, compared with natural volcanic rocks, the modified material exhibits increased specific surface area, pore volume, and active adsorption sites, leading to a significant improvement in NH_4^+-N adsorption capacity from 1.817 to 3.690 mg·g^{-1}. The adsorption of ammonia nitrogen onto the modified material follows the second-order kinetic model and Freundlich model, and is an endothermic and entropy-driven process, with the spontaneity increasing with temperature. The material exhibits stronger binding affinity for ammonia nitrogen under neutral and alkaline conditions, and coexisting cations exerted only limited interference on the adsorption performance under the tested conditions. The main adsorption mechanism involves a combination of electrostatic interaction and coordination bonding.

Furthermore, the saturated volcanic rock@FeOOH exhibited low desorption efficiency in deionized water and alkaline solutions, and showed a low cumulative release rate (1.4%) after nine soil column leaching events—significantly lower than that of unmodified volcanic rock (4.2%). This demonstrates the effectiveness of FeOOH modification in improving the slow-release property, highlighting its potential as a slow-release fertilizer for agricultural applications. Overall, the synthesized volcanic rock@FeOOH can serve as a promising adsorbent for ammonia nitrogen capture through FeOOH loading, and shows potential for the recovery and resource utilization of ammonia nitrogen from wastewater. This study focused on the adsorption mechanism and the slow-release fertilizer potential of the spent adsorbent; real-wastewater validation, regeneration cycles, and field-scale risk assessment should be addressed in future work.

Supplementary Materials: The following supporting information can be downloaded at: https://www.mdpi.com/article/10.3390/w18232912/s1, Figure S1: Effect of adsorbent dose on the adsorption capacity and the removal efficiency of NH_4^+-N by volcanic rock and volcanic rock@FeOOH. (C_0 = 10 mg·L^{-1}, 25°C, 120 min); Figure S2: Diagram of soil column leaching test device; Table S1: Atomic proportional composition (at%) of volcanic rock, volcanic rock@FeOOH before adsorption, and volcanic rock@FeOOH after adsorption (full spectrum of XPS); Table S2: Relative content (at%) of Fe and O of volcanic rock, volcanic rocks@FeOOH before adsorption, and volcanic rock@FeOOH after adsorption (deconvoluted spectra of XPS); Table S3: Desorption rates (%) of volcanic rock and volcanic rock@FeOOH in different desorption fluids; Section S2: Detailed experimental parameters and procedures for soil column leaching experiment.

Author Contributions: Conceptualization, X.R. and D.M.; methodology, Y.L.; validation, J.H.; formal analysis, Y.L., X.R. and J.H.; investigation, Y.L., J.C. and Z.T.; data curation, Y.L., J.C. and Z.T.; writing—original draft preparation, Y.L.; writing—review and editing, X.R.; visualization, Y.L. and X.R.; supervision, D.M.; project administration, D.M. All authors have read and agreed to the published version of the manuscript.

Funding: This research was funded by the Bagui Youth Top Talent Program of Guangxi (GuiRenCaiBan [2024]1).

Data Availability Statement: All data supporting the findings of this study are included in the article and its Supplementary Materials. Further inquiries may be directed to the corresponding author.

Conflicts of Interest: The authors declare no conflicts of interest.

References

1. Ma, H.; Chen, G.; Huang, F.; Li, Y.; Zhang, L.; Jin, Y. Catalytic ozonation of ammonia nitrogen removal in wastewater: A review. *J. Water Process Eng.* **2023**, *52*, 103542. [CrossRef]
2. Wang, B.; Qiao, X.; Hou, F.; Liu, T.; Pang, H.; Guo, Y.; Guo, J.; Peng, Y. Pilot-scale demonstration of a novel process integrating partial nitritation with simultaneous anammox, denitrification and sludge fermentation (PN + ADSF) for nitrogen removal and sludge reduction. *Sci. Total Environ.* **2022**, *815*, 152835. [CrossRef] [PubMed]
3. Zhang, Y.; Yin, S.; Li, H.; Liu, J.; Li, S.; Zhang, L. Treatment of ammonia-nitrogen wastewater by the ultrasonic strengthened break point chlorination method. *J. Water Process Eng.* **2022**, *45*, 102501. [CrossRef]
4. Zhu, L.; Dong, D.; Hua, X.; Guo, Z.; Liang, D. Ammonia nitrogen removal from acetylene purification wastewater from a PVC plant by struvite precipitation. *Water Sci. Technol.* **2016**, *74*, 508–515. [CrossRef]
5. Chen, T.-L.; Chen, L.-H.; Lin, Y.J.; Yu, C.-P.; Ma, H.; Chiang, P.-C. Advanced ammonia nitrogen removal and recovery technology using electrokinetic and stripping process towards a sustainable nitrogen cycle: A review. *J. Clean. Prod.* **2021**, *309*, 127369. [CrossRef]
6. Zhu, Y.; Chang, H.; Yan, Z.; Liu, C.; Liang, Y.; Qu, F.; Liang, H.; Vidic, R.D. Review of ammonia recovery and removal from wastewater using hydrophobic membrane distillation and membrane contactor. *Sep. Purif. Technol.* **2024**, *328*, 125094. [CrossRef]
7. Han, B.; Butterly, C.; Zhang, W.; He, J.; Chen, D. Adsorbent materials for ammonium and ammonia removal: A review. *J. Clean. Prod.* **2021**, *283*, 124611. [CrossRef]
8. Zhou, H.-D.; Wang, C.-Y.; Wang, Q.; Xu, B.-X.; Zhu, G. Efficiency, mechanism and application prospect of ammonium adsorption and desorption over a sodium-acetate-modified synthetic zeolite. *RSC Adv.* **2024**, *14*, 17843–17854. [CrossRef] [PubMed]
9. Faccini, B.; Giuseppe, D.; Ferretti, G.; Coltorti, M.; Colombani, N.; Mastrocicco, M. Natural and NH_4^+-enriched zeolitite amendment effects on nitrate leaching from a reclaimed agricultural soil (ferrara province, italy). *Nutr. Cycl. Agroecosyst.* **2018**, *110*, 327–341. [CrossRef]
10. Shao, Q.; Zhang, Y.; Liu, Z.; Long, L.; Liu, Z.; Chen, Y.; Hu, X.-M.; Lu, M.; Huang, L.-Z. Phosphorus and nitrogen recovery from wastewater by ceramsite: Adsorption mechanism, plant cultivation and sustainability analysis. *Sci. Total Environ.* **2022**, *805*, 150288. [CrossRef] [PubMed]
11. Sun, Q.; Zhou, H.; Xu, C.; Ba, Y.; Geng, Z.; She, D. Effective adsorption of ammonium nitrogen by sulfonic-humic acid char and assessment of its recovery for application as nitrogen fertilizer. *Sci. Total Environ.* **2023**, *867*, 161591. [CrossRef] [PubMed]
12. Zhao, Z.; Wang, B.; Feng, Q.; Chen, M.; Zhang, X.; Zhao, R. Recovery of nitrogen and phosphorus in wastewater by red mud-modified biochar and its potential application. *Sci. Total Environ.* **2023**, *860*, 160289. [CrossRef] [PubMed]
13. Feng, L.; Qiu, T.; Liu, C. Study on adsorption of ammonia nitrogen by sodium-modified kaolin at calcination temperature. *Environ. Sci. Pollut. Res.* **2023**, *30*, 97063–97077. [CrossRef] [PubMed]
14. Shi, C.; Gao, M.; Huang, X.; Wang, X.; Jiang, J.; Zhang, Y. Preparation of magnesium-modified steel slag and its adsorption performance for simultaneous removal of nitrogen and phosphorus from water. *Colloids Surf. A* **2024**, *702*, 135068. [CrossRef]
15. Zhou, H.; Ou, L. Adsorption of ammonia nitrogen in wastewater by tailing loaded manganese oxide material. *Inorg. Chem. Commun.* **2022**, *144*, 109886. [CrossRef]
16. Chi, R.; Wei, Z.; Gong, L.; Zhang, G.; Wen, D.; Li, W. The study of nitrogen and phosphorus removal efficiency in urbanized river systems using artificial wetland systems with different substrates. *Water* **2024**, *16*, 3309. [CrossRef]
17. Wang, X.-G.; Qin, J.-W.; Zheng, X.-M.; Xie, L.; Li, W. Analysis of the removal effect of modified volcanic rocks on ammonia nitrogen in water. *Chin. J. Appl. Chem.* **2024**, *41*, 1193. [CrossRef]
18. Huang, Z.; Chang, B.; Tang, Y.; Li, Q.; Zhang, Z.; Wei, S.; Chang, X.; Yang, Y.; Xu, C.; Hu, F.; et al. Co-adsorption performance and mechanism of ammonium and phosphate by iron-modified biochar in water. *J. Water Process Eng.* **2024**, *67*, 106209. [CrossRef]
19. Xu, Q.; Li, W.; Ma, L.; Cao, D.; Owens, G.; Chen, Z. Simultaneous removal of ammonia and phosphate using green synthesized iron oxide nanoparticles dispersed onto zeolite. *Sci. Total Environ.* **2020**, *703*, 135002. [CrossRef] [PubMed]
20. Duranoğlu, D.; Trochimczuk, A.W.; Beker, U. Kinetics and thermodynamics of hexavalent chromium adsorption onto activated carbon derived from acrylonitrile-divinylbenzene copolymer. *Chem. Eng. J.* **2012**, *187*, 193–202. [CrossRef]
21. Wang, Q.; Hu, J.; Wu, Z.; Wang, Z.; Meng, F.; Wu, Z.; Lin, Z.; Li, X. Impact of silicate on the microstructure of β-FeOOH and its adsorption of As. *Sep. Purif. Technol.* **2025**, *354*, 129221. [CrossRef]
22. Cheburet, F.J.; Kiptoo, J.K.; Wanyika, H.N. Efficient release of urea with amorphous silica from pumice rock. *Sci. Rep.* **2025**, *15*, 35139. [CrossRef] [PubMed]
23. Bagci, C.; Tameni, G.; Elsayed, H.; Bernardo, E. Sustainable manufacturing of new construction material from alkali activation of volcanic tuff. *Mater. Today Commun.* **2023**, *36*, 106645. [CrossRef]
24. Otieno, S.O.; Kengara, F.O.; Kowenje, C.O.; Mokaya, R. Hydrothermal synthesis of zeolites using silica extracted from tropical volcanic ash. *Mater. Adv.* **2023**, *4*, 2292–2300. [CrossRef]
25. Villalba, J.C.; Constantino, V.R.L.; Anaissi, F.J. Iron oxyhydroxide nanostructured in montmorillonite clays: Preparation and characterization. *J. Colloid Interface Sci.* **2010**, *349*, 49–55. [CrossRef] [PubMed]

26. Qin, R.; Hao, L.; Li, J. Acid-assisted one-step In-situ polymerization synthesis of PANI/α-Fe_2O_3/β-FeOOH composites and its formation mechanism. *J. Inorg. Organomet. Polym. Mater.* **2020**, *30*, 4452–4458. [CrossRef]
27. Zhang, D.; Liu, J.; Zhu, S.; Xiong, H.; Xu, Y. Adsorption removal of Cr(VI) by isomeric FeOOH. *Water Sci. Technol.* **2019**, *80*, 300–307. [CrossRef] [PubMed]
28. Lin, F.; Lien, H.-L.; Shih, Y.; Ta Fu Kuo, D. Effect of surfactants and implementation strategies for the pentachlorophenol degradation with Ni/Fe bimetallic nanoparticles in soil. *Sep. Purif. Technol.* **2025**, *354*, 129097. [CrossRef]
29. Wolski, L.; Sobczak, I.; Ziolek, M. Variability of surface components in gold catalysts—The role of hydroxyls and state of gold on activity and selectivity of Au-Nb_2O_5 and Au-$ZnNb_2O_6$ in methanol oxidation. *J. Catal.* **2017**, *354*, 100–112. [CrossRef]
30. Xu, X.; Gao, B.-Y.; Yue, Q.-Y.; Zhong, Q.-Q. Preparation and utilization of wheat straw bearing amine groups for the sorption of acid and reactive dyes from aqueous solutions. *J. Hazard. Mater.* **2010**, *182*, 1–9. [CrossRef] [PubMed]
31. Wang, G.; Su, X.; Hua, Y.; Ma, S.; Wang, J.; Xue, X.; Tao, Q.; Komarneni, S. Kinetics and thermodynamic analysis of the adsorption of hydroxy-Al cations by montmorillonite. *Appl. Clay Sci.* **2016**, *129*, 79–87. [CrossRef]
32. Sağ, Y.; Kutsal, T. Determination of the biosorption heats of heavy metal ions on *Zoogloea ramigera* and *Rhizopus arrhizus*. *Biochem. Eng. J.* **2000**, *6*, 145–151. [CrossRef] [PubMed]
33. Zhang, Z.; Zhao, L.; Chen, J.; Wang, Y.; Liu, Y.; Hou, X.; Qu, J.; Lv, C.; Hu, Q. Ultra-strong adsorption of ammonia nitrogen from low-temperature and complex systems by prussian blue analogue. *Sep. Purif. Technol.* **2025**, *355*, 129700. [CrossRef]
34. Zhang, Y.; Yu, F.; Cheng, W.; Wang, J.; Ma, J. Adsorption equilibrium and kinetics of the removal of ammoniacal nitrogen by zeolite X/activated carbon composite synthesized from elutrilithe. *J. Chem.* **2017**, *2017*, 1936829. [CrossRef]
35. El-Ghobashy, M.A.; Khamis, M.M.; Elsherbiny, A.S.; Salem, I.A. Selective removal of ammonia from wastewater using Cu(II)-loaded amberlite IR-120 resin and its catalytic application for removal of dyes. *Environ. Sci. Pollut. Res.* **2023**, *30*, 106822–106837. [CrossRef] [PubMed]
36. Peng, L.; Yin, T.; Song, Z.; Xiong, S.; Liu, R.; You, J.; Huang, Q. Superior ammonia nitrogen adsorption capacity and reusability biochar microsphere applied in live fish transportation. *Chem. Eng. J.* **2025**, *514*, 163261. [CrossRef]
37. Li, Z.; Lu, J.; Zhang, T.; Liu, Y.; Pan, R.; Fu, Q.; Liu, X.; Mao, S.; Xu, B. Pyrazine-based iron metal organic frameworks (Fe-MOFs) with modulated O-Fe-N coordination for enhanced hydroxyl radical generation in fenton-like process. *J. Colloid Interface Sci.* **2024**, *674*, 279–288. [CrossRef] [PubMed]
38. Sato, N.; Aoyama, Y.; Yamanaka, J.; Toyotama, A.; Okuzono, T. Particle adsorption on hydrogel surfaces in aqueous media due to van der waals attraction. *Sci. Rep.* **2017**, *7*, 6099. [CrossRef] [PubMed]
39. Liu, Q.; Liu, B.; Zhang, Y.; Hu, T.; Lin, Z.; Liu, G.; Wang, X.; Ma, J.; Wang, H.; Jin, H.; et al. Biochar application as a tool to decrease soil nitrogen losses (NH_3 volatilization, N_2O emissions, and N leaching) from croplands: Options and mitigation strength in a global perspective. *Glob. Change Biol.* **2019**, *25*, 2077–2093. [CrossRef] [PubMed]

Disclaimer/Publisher's Note: The statements, opinions and data contained in all publications are solely those of the individual author(s) and contributor(s) and not of MDPI and/or the editor(s). MDPI and/or the editor(s) disclaim responsibility for any injury to people or property resulting from any ideas, methods, instructions or products referred to in the content.